Hydrological, meteorological and watershed controls on the water balance of thermokarst lakes between Inuvik and Tuktoyaktuk, Northwest Territories, Canada

Evan J. Wilcox[1], Brent B. Wolfe[1], and Philip Marsh[1]

[1]Department of Geography and Environmental Studies, Wilfrid Laurier University, Waterloo, N2L3C5, Canada
Correspondence: E. J. Wilcox (evan.j.wilcox@gmail.com)

Abstract. Thermokarst lake water balances are becoming increasingly vulnerable to change in the Arctic as air temperature increases and precipitation patterns shift. In the tundra uplands east of the Mackenzie Delta in the Northwest Territories, Canada, previous research has found that lakes responded non-uniformly to year-to-year changes in precipitation, suggesting that lake and watershed properties mediate the response of lakes to climate change. To investigate how lake and watershed properties and meteorological conditions influence the water balance of thermokarst lakes in this region, we sampled 25 lakes for isotope analysis five times in 2018, beginning before snowmelt on May 1 and sampling throughout the remainder of the ice-free season. Water isotope data were used to calculate the ratio of evaporation-to-inflow (E/I) and the average isotope composition of lake source water (δ_I). We identified four distinct water balance phases as lakes responded to seasonal shifts in meteorological conditions and hydrological processes. During the freshet phase from May 1 to June 15, the median E/I ratio of lakes decreased from 0.20 to 0.13 in response to freshet runoff and limited evaporation due to lake ice presence that persisted for the duration of this phase. During the following warm, dry, and ice-free period from June 15 to July 26, designated the evaporation phase, the median E/I ratio increased to 0.19. During the brief soil wetting phase, E/I ratios did not respond to rainfall between July 26 and August 2, likely because watershed soils absorbed most of the precipitation which resulted in minimal runoff to lakes. The median E/I ratio decreased to 0.11 after a cool and rainy August, identified as the recharge phase. Throughout the sampling period, δ_I remained relatively stable and most lakes contained a greater amount of rainfall-sourced water than snow-sourced water, even after the freshet phase due to snowmelt bypass. The range of average E/I ratios we observed at lakes (0.00 – 0.43) was relatively narrow and low compared to thermokarst lakes in other regions, likely owing to the large watershed area to lake area ratio (WA/LA), efficient preferential flow pathways for runoff, and a shorter ice-free season. Lakes with smaller WA/LA tended to have higher E/I ratios ($R^2 = 0.74$). An empirical relationship between WA/LA and E/I was derived and used to predict the average E/I ratio of 7340 lakes in the region, which identified that these lakes are not vulnerable to desiccation, given that all predicted average E/I ratios were <0.33. If future permafrost thaw and warming cause less runoff to flow into lakes, we expect that lakes with smaller WA/LA will be more influenced by increasing evaporation, while lakes with larger WA/LA will be more resistant to lake-level drawdown.

25 However under wetter conditions, lakes with larger WA/LA will likely experience greater increases in lake level and could be more susceptible to rapid drainage~~as a result~~.

1 Introduction

Thermokarst lakes are common features in ice-rich permafrost terrain, occupying up to 25% of the land area (Woo, 2012). The water balance of thermokarst lakes are changing as arctic warming causes precipitation to shift from snowfall to rainfall
30 (Bintanja and Andry, 2017; MacDonald et al., 2021), permafrost thaw alters the hydrological connectivity of lake watersheds (Wolfe et al., 2011; Walvoord and Kurylyk, 2016; Tananaev and Lotsari, 2022; Koch et al., 2022), longer ice-free periods increase evaporation (Prowse et al., 2011; Arp et al., 2015), and increased vegetation growth changes snow redistribution and snowmelt timing (Sturm et al., 2001; Essery and Pomeroy, 2004; Pomeroy et al., 2006). In many regions, expansion and contraction of thermokarst lakes has been observed demonstrating that lake water balances are not responding uniformly to
35 climate change (Smith et al., 2005; Plug et al., 2008; Marsh et al., 2009; Arp et al., 2011; Jones et al., 2011; Andresen and Lougheed, 2015; Travers-Smith et al., 2021).

Previous studies have demonstrated that knowledge of meteorological conditions and lake and watershed attributes, and their influence on lake water balance, can explain why thermokarst lakes react non-uniformly to climate change (Brock et al., 2009; Wolfe et al., 2011; Turner et al., 2014; Nitze et al., 2017; Wan et al., 2020)(Wolfe et al., 2011; Turner et al., 2014; Nitze et al., 2017; Wan et al., 2020).
40 Key drivers of lake water balances include the relative size of a lake within its watershed (Watershed Area/Lake Area, WA/LA), rainfall and snowfall patterns, permafrost dynamics, wildfire, vegetation cover, and ice-free season length (Turner et al., 2014; Arp et al., 2015; MacDonald et al., 2017; Wan et al., 2020). For example, Turner et al. (2014) found that thermokarst lakes in Old Crow Flats, Yukon, with increased evaporation-inflow ratios (E/I) tended to have smaller WA/LA ratios, reflecting the control of watershed area on the amount of inflow a lake receives. Arp et al. (2015) found that lakes in the Alaskan Coastal Plain
45 with bedfast ice became ice-free sooner than lakes with floating ice, causing bedfast lakes to lose more water to evaporation as a result of a longer ice-free season.

In several studies, water isotope (δ^{18}O and δ^2H) analysis has been the primary method used to efficiently characterize the water balance of a large number of thermokarst lakes because the isotope composition provides an integrated measure of influential hydrological processes (Edwards et al., 2004)(Gibson, 2002; Edwards et al., 2004; Turner et al., 2014; Narancic et al.,
50 2017). Two key metrics of lake water balance modelled using water isotope data include the average isotope composition of lake source waters (δ_I), which can then be related to the measured isotope composition of different water sources (Yi et al., 2008) and the ratio of evaporation to inflow evaporation-to-inflow (E/I) (Gibson et al., 1993). Sampling lake water for isotope analysis multiple times throughout the year provides data to assess the response of lake water balances to different hydrological processes, which can be related to meteorological conditions and compared to lake and watershed attributes. Recently, MacDonald
55 et al. (2017) compared E/I and δ_I of thermokarst lakes from six regions in northern North America and found a wide range of water balances that were influenced by local meteorological conditions, permafrost extent and vegetation characteristics.

In some locations, such as the Alaskan Coastal Plain, E/I ratios were mostly below 0.2, whereas lakes in the Hudson Bay Lowlands of northeastern Manitoba typically possessed E/I ratios >0.5, with some lakes trending towards desiccation.

This study aims to evaluate how meteorological conditions, hydrological processes, and lake and watershed attributes influence the δ_I and E/I of lakes located in the tundra uplands east of the Mackenzie Delta in the Northwest Territories, Canada (Figure 1). A previous study in this region showed that only 25% of pre-snowmelt lake water is replaced by freshet on average, because snowmelt bypass leads to minimal mixing between freshet and pre-snowmelt lake water (Bergmann and Welch, 1985; Wilcox et al., 2022). Snowmelt bypass occurs when less dense (~0°C) freshet runoff flows underneath lake ice and passes through a lake without mixing with and replacing the deeper and denser (<4°C) lake water. With this study we explore whether snowmelt bypass influences summertime lake water balances, given that in other regions thermokarst lakes are prone to desiccation when they retain little snowmelt (Bouchard et al., 2013). We also investigate how watershed characteristics that have been identified to influence lake water balance in other regions, such as WA/LA, influence lake water balances. We then use the relationships relationship found between average E/I and watershed characteristics to predict average E/I for all lakes in the region and assess their vulnerability to climate change.

2 Study Area

The thermokarst lakes in this study are located in the tundra uplands east of the Mackenzie Delta in the northwest region of the Northwest Territories, Canada (Figure 1). The landscape is comprised of rolling hills and has been shaped by the thaw of ice-rich permafrost, evidenced by the thousands of thermokarst lakes in the region (Rampton, 1988; Burn and Kokelj, 2009). Hillslopes are well-drained by the network of peat channels that facilitate subsurface flow between mineral earth hummocks (Quinton and Marsh, 1998), while flatter areas are typically drained by high-centred ice-wedge polygons (Burn and Kokelj, 2009). Vegetation consists of tall shrub (>1 m), low-shrub low shrub (~0.5 m), and shrub-free landcover types containing lichen, moss, and tussocks (Lantz et al., 2010; Grünberg et al., 2020).

We selected 25 lakes to cover that span a range of watershed sizes , (6.45 to 203.56 ha) and lake surface areas, among other characteristics, along a ~70 km stretch of the Inuvik - Tuktoyaktuk Highway (Figure 1). All lakes we selected were either headwater lakes or downstream of lakes that we sampled. The average area of the studied lakes is 10.43 ha (0.37 to 90.48 ha) and the average maximum depth is 2.28 m (1.02 to 4.14 m) (, Table 1). Twenty Nineteen of the lakes are headwater lakes and the other five six lakes are downstream of other sampled lakes (Table 1). All lakes have a defined outlet channel and many lakes have defined channelized inflows from their watersheds in the form of small ephemeral streams or ice-wedge polygon troughs.

3 Methods

3.1 Lake water and precipitation sampling and analysis of isotope data

Water samples from the 25 thermokarst lakes were collected on five days (May 1, June 15, July 26, August 2, September 3) during 2018 for water isotope analysis. Samples were collected on May 1 through a hole augured through the ice in the centre of

Table 1. Lake and watershed attributes and ~~isotope derived~~ isotope-derived hydrological indicators for all lakes.

Lake	Latitude (dec deg.)	Lake Depth (m)	Lake Elevation (m asl)	Ice-wedge Polygon Coverage (% Watershed)	Watershed Slope (°)	Lake Area (ha)	Watershed Area (ha)	WA/LA	Headwater Lake?	Upstream Lake(s)	Drainage Density (m ha^{-1})	E/I Average	δ_I Average (‰ $\delta^{18}O_I$)
7	68.557	2.24	89.0	0.00	1.30	2.94	6.45	2.62	yes	none	0.00	0.28	-19.82
8	68.559	2.30	88.9	0.00	2.63	2.07	15.67	4.41	no	7	0.00	0.21	-20.58
9	68.564	1.02	86.4	29.84	1.20	59.56	203.56	3.77	no	7,8,10	22.28	0.40	-18.19
10	68.576	1.65	87.9	5.17	1.42	90.48	168.58	1.86	yes	none	7.40	0.35	-18.85
11	68.604	1.91	82.7	2.53	2.10	1.26	21.76	17.32	yes	none	12.68	0.04	-19.84
12	68.613	2.79	90.8	0.00	2.45	8.19	23.05	2.81	~~yes~~ no	none	0.51	0.43	-21.84
14	68.789	1.42	51.9	8.07	3.01	10.65	60.64	5.70	yes	none	1.24	0.09	-20.35
15	68.795	1.57	57.2	1.62	2.73	5.98	29.83	4.99	yes	none	0.00	0.17	-18.81
16	68.805	3.18	51.5	12.57	4.04	1.23	19.75	16.02	yes	none	4.86	0.04	-19.65
17	68.836	1.09	39.1	8.23	4.38	3.27	39.88	12.20	yes	none	11.53	0.08	-20.21
19	68.882	2.46	39.2	4.91	4.27	5.50	38.98	7.09	yes	none	5.79	0.10	-19.69
20	68.885	2.69	36.7	2.76	4.69	2.17	19.93	9.18	yes	none	3.04	0.10	-19.33
21	68.887	1.78	35.5	1.87	5.33	2.75	10.91	10.31	no	20	6.86	0.16	-20.07
22	68.907	3.66	33.6	4.11	5.33	3.41	23.67	18.25	no	23,24	6.12	0.12	-19.75
23	68.910	3.02	34.9	1.22	5.35	1.83	22.73	20.40	no	24	4.88	0.04	-19.22
24	68.911	3.02	38.3	4.49	4.69	0.37	11.10	30.10	yes	none	9.69	-0.01	-19.15
26	68.918	1.47	38.4	4.71	4.69	4.68	17.89	3.83	yes	none	0.00	0.25	-18.45
27	68.921	3.10	45.4	0.00	6.21	1.28	8.57	6.70	yes	none	0.00	0.17	-20.52
28	68.933	2.24	24.1	9.58	4.66	2.32	92.08	39.69	yes	none	22.73	0.01	-19.28
49	69.119	2.18	8.6	4.06	3.18	18.20	46.23	2.54	yes	none	0.79	0.31	-17.45
50	69.123	1.65	8.3	2.92	3.85	8.70	31.92	3.67	yes	none	0.00	0.23	-17.53
51	69.142	2.31	3.8	0.00	4.90	2.29	12.01	5.26	yes	none	0.00	0.19	-18.46
52	69.144	4.14	6.3	1.26	3.93	24.32	49.92	2.05	yes	none	0.00	0.32	-17.01
53	69.184	2.29	4.8	8.71	6.54	0.46	11.21	24.21	yes	none	10.05	0.13	-19.38
55	69.215	1.83	2.3	0.00	2.12	1.61	8.11	5.03	yes	none	0.00	0.18	-17.71
Min	68.557	1.02	2.3	0.00	1.2	0.37	6.45	1.86	n/a	n/a	0.00	-0.01	-21.84
Avg.	68.871	2.28	43.4	4.75	3.8	10.43	39.78	10.40	n/a	n/a	5.218	0.16	-19.25
Max	69.215	4.14	90.8	29.84	6.54	90.48	203.56	39.69	n/a	n/a	22.73	0.43	-17.01
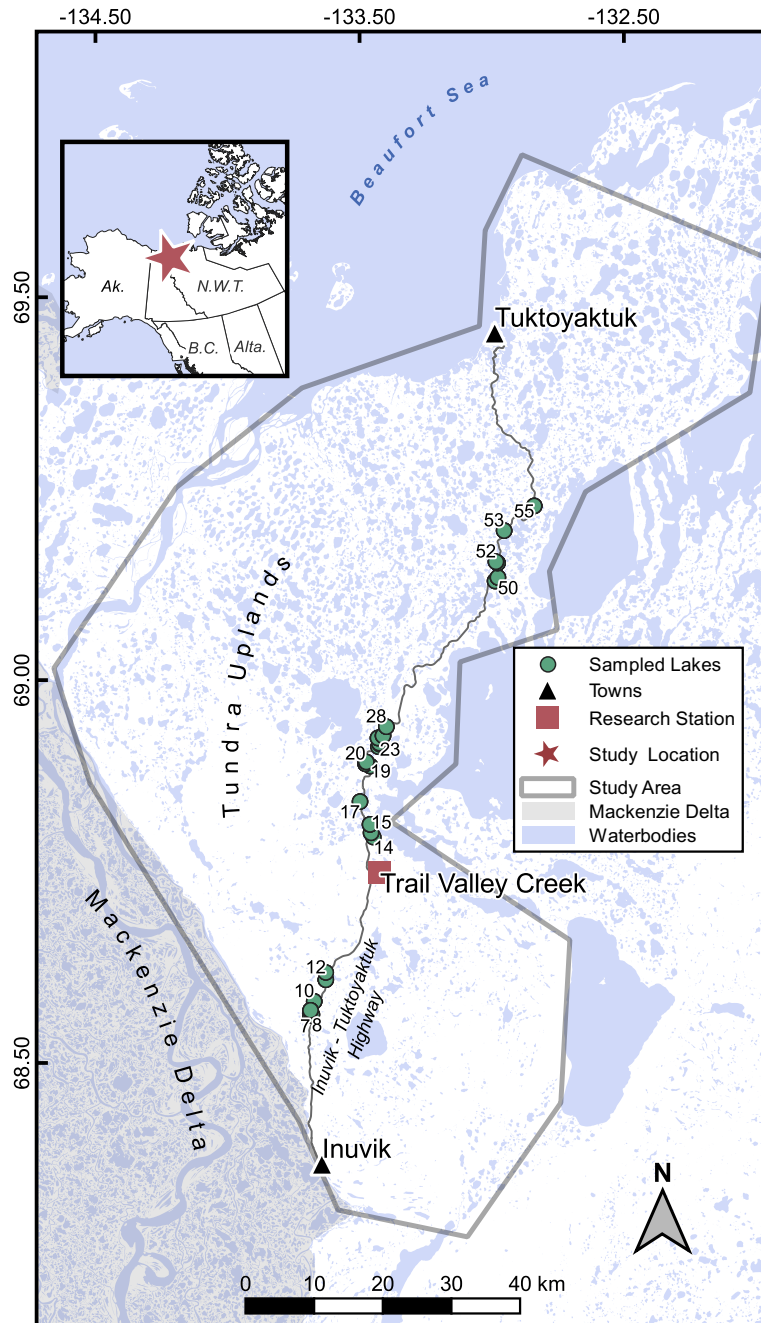
Figure 1. Study area showing locations of thermokarst lakes where water samples for isotope analysis were ~~taken~~obtained. The ~~locations of the meteorological station~~ study location relative to northwestern North America is shown ~~in Inuvik and the Trail Valley Creek research station~~ inset map. Not all lakes are ~~also shown~~labeled on the map, but lakes are numbered sequentially from south to north.

each lake to capture the pre-snowmelt lake water balance conditions. The May 1 samples also represent the hydrological status of lakes during the freeze-up period of 2017, since virtually no hydrological activity occurs during the winter months due to the complete freezing of the soil and lake surface. Because May 1 water samples were influenced by fractionation that occurred during lake ice formation, the isotope compositions were corrected to represent the isotope composition of the lake before lake ice formation took place (Wilcox et al., 2022). Lake water samples were corrected for ice fractionation by estimating the fraction of lake water that had been frozen and the corresponding amount of isotopic depletion of lake water that would have occurred assuming the lake was a closed system, following Ferrick et al. (2002). June 15 was chosen as it marked the first day of the ice-free season for most lakes and was intended to capture the influence of snowmelt bypass, a phenomenon where snowmelt runoff to flows underneath lake ice and out of lakes without mixing with pre-snowmelt lake waters (Bergmann and Welch, 1985). however the southernmost lakes (Lakes 7-12) became ice-free on June 7, and some of the northernmost lakes (Lakes 49-55) became ice-free on June 17 or June 18. More information about ice-correction and the response of lakes to snowmelt bypass is provided by Wilcox et al. (2022). Next, samples were obtained on July 26 to capture the effects of evaporation and rainfall in the early open-water season, and before a large, forecasted rainfall event occurred. Samples were then collected on August 2 to capture the influence of the a week-long rainy period following the sampling date on July 26. Samples were lastly taken on September 3 to assess lake water balance response to the relatively rainy and cool August weather prior to freeze-up. The four time periods between the five sampling dates are identified as "P1" (May 1 to Jun. 15), "P2" (Jun. 15 to Jul. 26), "P3" (Jul. 26 to Aug. 2), and "P4" (Aug. 2 to Sept. 3).

From June 15 onward, water samples were collected at the shoreline of each lake where water was freely circulating. Samples of end-of-winter snow and open-water season rainfall were obtained to determine the average isotope composition of rain (δ_R) and snow (δ_S). Snow samples (n = 11) were collected from the region in late April by taking a vertical core of snow the end-of-winter snowpack using a tube, completely melting the snow in a sealed plastic bag, and then filling a sampling bottle with the melted snow. Rainfall (n = 13) was collected between May and September in Inuvik using a clean high density polyethylene container, which was then transferred into a sample bottle shortly after precipitation ceased. All samples were stored in 30 mL high-density polyethylene bottles. A Los Gatos Research (LGR) Liquid Water Isotope Analyser, model T-LWIA-45-EP was used to measure the ratio of $^{18}O/^{16}O$ and $^2H/^1H$ in each sample at the Environmental Isotope Laboratory at the University of Waterloo. Vienna Mean Standard Ocean Water (VSMOW) and Vienna Standard Light Antarctic Precipitation (VSLAP) standards provided by LGR were used to calibrate the instrument. VSMOW and VSLAP standards were used during the analysis to check the calibration of the instrument. Isotope compositions are expressed in standard δ-notation, such that:

$$\delta_{sample} = \frac{R_{sample}}{R_{VSMOW}} - 1 * 10^3 - 1 \tag{1}$$

where R represents the ratio of $^{18}O/^{16}O$ or $^2H/^1H$, and VSMOW represents Vienna Mean Standard Ocean Water. Isotope values are normalized for Standard Light Antarctic Precipitation to $\delta^{18}O$ = -55.5 ‰ and δ^2H = -428 ‰ (Coplen, 1996). Each isotope measurement consisted of 8 injections of roughly 1000nL sample volume, with the first 2 injections being discarded and the remaining 6 injections averaged to produce the measurement value. All samples were pre-filtered to 0.45 micron into 12x32mm septum vials. Every fifth sample was run through the analyzer a twice measured a second time to determine the analytical
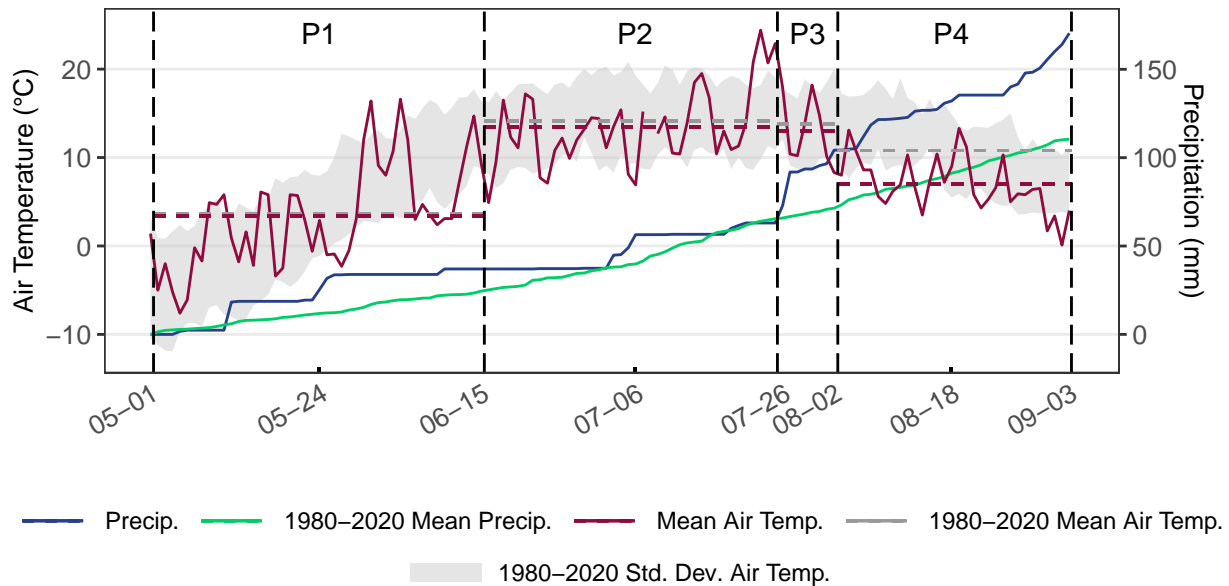
Figure 2. Air temperature and cumulative precipitation during the sampling period and the 1980-2020 mean, as recorded at Inuvik (WMO ID: 71364) (Figure 1). Meteorological data were retrieved from Environment and Climate Change Canada (2019). The five days when water samples were taken from lakes are shown by the vertical dotted dashed lines. The periods between the sampling dates are labeled P1, P2, P3, and P4. Mean daily air temperature for 2018 and 1980-2020 for each period is indicated by the horizontal dashed lines.

uncertainties, which were ±0.1‰ for δ^{18}O and ±0.6‰ for δ^2H, calculated as two standard deviations away from the difference between the duplicate samples. VSMOW and Vienna Standard Light Antarctic Precipitation (VSLAP) standards provided by LGR were used to calibrate the instrument initially, and VSMOW and VSLAP standards were analyzed intermittently
125   throughout the sample run to confirm the accuracy of the instrument.

3.2   Isotope framework, δ_I and E/I

The isotope data were initially described and interpreted with respect to an 'isotope framework' that consists of two fundamental linear relationships that form when isotope data is plotted with δ^{18}O on the x-axis and δ^2H on the y-axis ('δ-^{18}O-δ^2H space'). The isotope composition of precipitation from anywhere in the world tends to plot closely to the Global Meteoric
130   Water Line (GMWL), a strong linear correlation in δ^{18}O-δ^2H space which is defined as $\delta^2 H = 8.0 * \delta^{18}O + 10$ (Craig, 1961). However, the slope and intercept of a Meteoric Water Line can vary for precipitation collected at a single location: the Local Meteoric Water Line (LMWL) represents the expected isotope composition of precipitation in the regionand was estimated a region. We estimated the LMWL for Inuvik using a linear regression through rainfall and snowfall isotope compositions. The average isotope composition of rainfall (δ_S and δ_R values) and snowfall (δ_S) were calculated by averaging the isotope
135   composition of all the rainfall and snowfall samples we collected respectively, with δ_P representing the average of δ_S and δ_R.

The LMWL equation we derived was $\delta^2 H = 7.1 * \delta^{18}O - 10.0$, which compared closely to the LMWL derived by Fritz et al. (2022), who used precipitation samples collected between 2015 and 2018 in Inuvik and estimated the Inuvik LMWL to be $\delta^2 H = 7.4 * \delta^{18}O - 6.7$. Both of these LMWL lines compare closely with the LMWL derived from the Global Network of Isotopes in Precipitation (GNIP) data set, which is comprised of precipitation samples in Inuvik between 1986 and 1989 and gives an LMWL of $\delta^2 H = 7.3 * \delta^{18}O - 3.6$ (IAEA/WMO, 2023). ~~We considered using the LMWL, δ_S, δ_P and δ_R values produced by Fritz et al. (2022), however we decided to use the LMWL we developed since it more closely represented the input waters during the study period, and~~ the δ_S, δ_P and δ_R values found by Fritz et al. (2022) were within 0.6‰ ($\delta^{18}O$) of the values we found.

Evaporated waters tend to plot along a Local Evaporation Line (LEL), which can be defined independent of measured lake water isotope compositions. Using this approach and for the case of a lake fed by waters of mean annual isotope composition of precipitation, the LEL was anchored at δ_P and the theoretical isotope composition of a lake at the point of total desiccation (δ^*), which is dependent on air temperature, relative humidity and the isotope composition of atmospheric moisture in the region (Gonfiantini, 1986). Along the LEL exists a useful reference point where the amount of evaporation a water body is experiencing is equal to the amount of water input, defined as δ_{SSL} (steady-state lake water isotope composition of a terminal basin). When lake water isotope compositions are plotted in δ-^{18}O-$\delta^2 H$ space, they typically plot near the LEL, with more evaporated lakes plotting closer to δ^* and less evaporated lakes plotting closer to δ_P. Lakes preferentially sourced by rainfall will tend to plot above the LEL, whereas lakes preferentially influenced by snowmelt will tend to plot below the LEL, owing to the normally distinctive isotope composition of rainfall and snowmelt.

Isotope compositions of the lakes were used to estimate the average isotope composition of source water (δ_I) and the ratio of evaporation-to-inflow (E/I), following , or $\delta^{18}O_I$ when referring to just ~~the~~ $\delta^{18}O$ ~~isotope concentrations~~). We followed the coupled isotope tracer method introduced by Yi et al. (2008) which ~~of~~ has been applied in a variety of northern environments (Turner et al., 2014; MacDonald et al., 2017; Remmer et al., 2020). locations (Turner et al., 2014; MacDonald et al., 2017; Remmer et al., 2020). Calculating δ_I using the approach of Yi et al. (2008) involves generating a lake-specific evaporation line for each lake water isotope composition. This approach assumes that all lakes tend towards δ^* as they evaporate, and the lake-specific evaporation line is defined as the line that intersects the lake water sample and δ^* in $\delta^{18}O$-$\delta^2 H$ space. δ_I is then calculated as the point of intersection between a lake-specific evaporation line and the LMWL.

We used these δ_I values to calculate the ratio of evaporation-to-inflow (E/I ~~was calculated as~~):

$$E/I = \frac{\delta_I - \delta_L}{\delta_E - \delta_L} \tag{2}$$

where δ_L is the isotope composition of the lake water and where δ_E is the isotope composition of evaporated vapour from the lake (Gonfiantini, 1986). More detailed information about the calculation of the isotope framework components, δ_I and E/I is provided in Appendix A.

3.3 Meteorological conditions and lake and watershed attributes

The end of winter snowpack at Trail Valley Creek contained 141 mm of snow water equivalent, similar to the 1991-2019 mean of 147 mm (Marsh et al., 2019). Air temperature at Inuvik was within a degree of the long-term mean during P1, P2 and P3, but P4 was 3.8°C cooler than the long-term mean (Figure 2). P1 and P2 experienced a combined 72.9 mm of rainfall, close to the long-term mean of 66.0 mm for this period, while P3 and P4 experienced 107.3 mm of rainfall, more than double the long-term mean of 45.0 mm for this period (Figure 2).

Multiple lake and watershed attributes for each lake were quantified for comparison with δ_I and E/I. Lake-specific properties included surface area, depth, latitude, and elevation, while watershed-specific properties included surface area, mean hillslope angle, drainage density, vegetation cover and ice-wedge polygon coverage (Table 1). Within each sampled lake watershed, the areas of ice-wedge polygons were identified visually from satellite imagery and digitized manually. Drainage density was calculated as the length of all flowpaths with a contributing area greater than 5000 m^2, and then divided by the total area of the watershed. A threshold of 5000 m^2 was chosen as this was roughly the threshold when water tracks became visible in optical satellite images. Vegetation height in each catchment watershed was quantified using the remote sensing vegetation height product produced by Bartsch et al. (2020), which provides vegetation height at 20 metre spatial resolution with a RMSE of 45 cm in vegetation height. All spatial analysis was carried out using ArcMap 10.7.1 (ESRI, 2019).

To evaluate whether lake and watershed properties were correlated with lake water balance components metrics derived from water isotope data, linear regressions between lake and watershed properties and E/I and δ_I were tested. Only correlations where p <0.01 were considered significant. The distribution of each variable was plotted on a histogram and data were mathematically transformed if the distribution was non-uniform. Statistical analysis was performed using R 4.1.0 (R Core Team, 2021).

We identified a strong relation A correlation was identified between WA/LA and average E/I and (R^2 = 0.82) and we used this relationship to predict average E/I for all lakes in the region . Watershed area was estimated for all lakes with areas >0.25 ha (n = 7454) in the study area outlined in Figure 1, Figure 1). Watershed area was estimated, including the 25 lakes sampled for isotope composition, by applying the D8 water routing algorithm (O'Callaghan and Mark, 1984) to the 2 m resolution the digital elevation model ArcticDEM (PGC, 2018). The ratio of WA/LA was calculated for each lake by dividing the total watershed area by the total area of the lake(s) in the watershed. In rare cases, watersheds were not delineated accurately and part of the watershed was clipped to the lake boundary; due to slight offsets between the lake layer and ArcticDEM. We rejected all watersheds where WA/LA <1.5, as all watersheds we inspected that met this criteria were improperly delineated due to the offset error just described. After rejecting all watersheds where WA/LA <1.5, a total of 7340 watersheds remained.
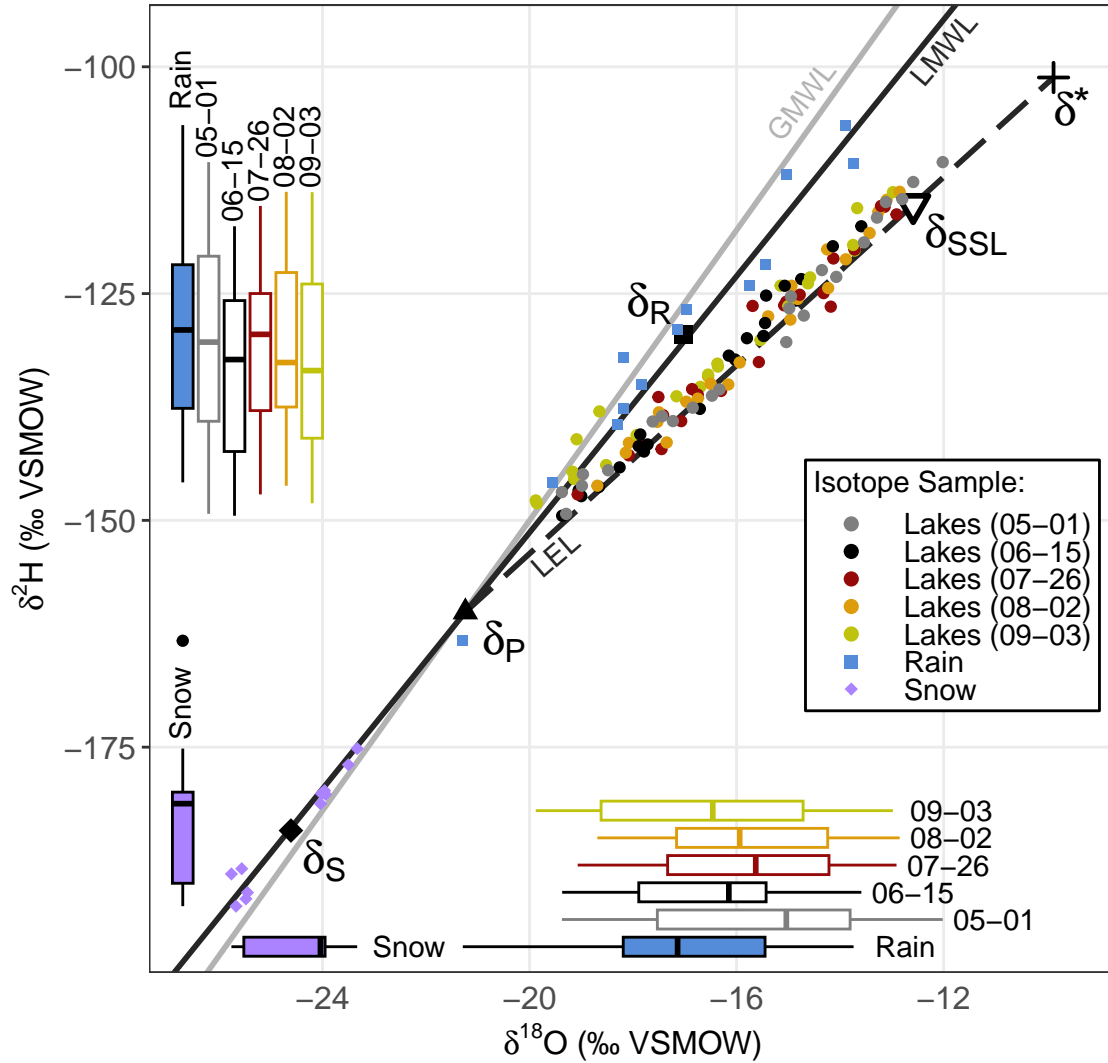
Figure 3. Isotope values and their respective ranges for all lake and precipitation samples are , with their respective ranges along each axis illustrated by boxplots, plotted in δ^{18}O-δ^2H space, as deviations per mil from Vienna Standard Mean Ocean Water (VSMOW). The Local Meteoric Water Line (LMWL, black solid line, $\delta^2H = 7.1 * \delta^{18}O - 10.0$) is calculated as a regression through snow samples collected throughout the study region and rain samples collected from Inuvik in 2018 (n = 24). The average isotope composition of end-of-winter snow samples (δ_S), rainfall samples (δ_R), and the average of δ_S and δ_R (δ_P) are labelled along the LMWL. The Local Evaporation Line (LEL, dark grey dashed line), $\delta^2H = 5.2 * \delta^{18}O - 48.9$ the Global Meteoric Water Line (GMWL, light solid grey line), the isotope composition of a waterbody at total desiccation (δ^*), and the point at which evaporation is equal to inflow (E/I = 1, δ_{SSL}) are added for reference.

4   Results

4.1   Seasonal evolution of lake water balances

Lake water isotope compositions span from near the LMWL to approaching δ_{SSL}, reflecting a range of lake water balance conditions (Figure 3). Lake water isotope compositions plot close to the LEL, indicating that the isotope framework has been
200   well estimated using the Trail Valley Creek meteorological data. No lakes along the LEL plot between δ_{SSL} and δ^*, indicating that E/I was <1 for all lake samples lakes sampled and lakes were not trending towards desiccation during any sampling episode. Some lakes above the LEL do plot past δ_{SSL}, however for lakes plotting above the LEL the point at which E/I = 1 is closer to δ^*. As expected, rain and snow samples isotope compositions plot in two distinct clusters along the isotopically-enriched and depleted segments of the LMWL, respectively, permitting rain-influenced and snow-influenced δ_I to be distinguished. Most
205   lakes plot slightly above the LEL, signifying that the δ_I of most lakes is more reflective of rain than snow.

We In general, we observed distinct shifts in lake water isotope composition along the LEL, $\delta^{18}O_I$ and E/I between sampling dates. Shifts in E/I between sampling dates were often more pronounced than shifts in $\delta^{18}O_I$. During P1 (May 1 to June 15), $\delta^{18}O$ decreased from a median of -15.04‰ (-17.53‰ to -13.81‰ inter-quartile range [IQR]) to -16.15‰ (-17.89‰ to -15.43‰ IQR) and δ^2H values decreased from -130.35‰ (-139.08‰ to -120.88‰ IQR) to -132.27‰ (-142.41‰ to -125.77‰ IQR) (Figure
210   3). At the same time, the range of $\delta^{18}O_I$ values decreased and the median decreased very slightly from -19.36‰ (-20.33‰ to -18.34‰ IQR) to -19.59‰ (-20.34‰ to -18.81‰ IQR) (Figure 4a). The median (and range) of E/I values also decreased during P1 from 0.20 (0.07 to 0.38 IQR) to 0.13 (0.07 to 0.18 IQR) (Figure 4b). The median reduction change in E/I was -0.08 (Figure 4c). The reduction in E/I values that occurred during P1 was larger than in any other period (Figure 4c).

During P2 (June 15 to July 26), lake water isotope compositions values increased slightly. The median $\delta^{18}O$ increased from
215   -16.15‰ (-17.89‰ to -15.43‰) to -15.63‰ (-17.33‰ to -14.22‰ IQR) and the median δ^2H increased from -132.27‰ (-142.41‰ to -125.77‰ IQR) to -129.50‰ (-137.90‰ to -124.99‰ IQR) (Figure 3). During P2, $\delta^{18}O_I$ increased very slightly from -19.59‰ (-20.34‰ to -18.81‰ IQR) to -19.35‰ (-20.34‰ to -18.55‰ IQR) (Figure 4a). The median E/I ratio increased from 0.13 (0.07 to 0.18 IQR) to 0.19 (0.09 to 0.31 IQR) (Figure 4b). The median increase in E/I was 0.06 (0.03 to 0.12 IQR) although three lakes experienced a decrease in E/I (Figure 4c).

220   Lake water isotope compositions values decreased marginally during P3 (July 26 to Aug 2). Median $\delta^{18}O$ decreased from -15.63‰ (-17.33‰ to -14.22‰ IQR) to -15.94‰ (-17.16‰ to -14.24‰ IQR) and median δ^2H decreased from -129.50‰ (-137.90‰ to -124.99‰ IQR) to -132.60‰ (-137.51‰ to -122.68‰ IQR) (Figure 3). E/I and $\delta^{18}O_I$ values also shifted minimally during P3. Median $\delta^{18}O_I$ decreased from -19.35‰ (-20.33‰ to -18.55‰ IQR) to -19.47‰ (-20.10‰ to -18.45‰ IQR) (Figure 4b). The median change in E/I was -0.01 (-0.06 to 0.02 IQR) with a near equal number of lakes experiencing an increase or
225   decrease in E/I (Figure 4c).

During P4 (August 2 to September 3), median $\delta^{18}O$ values decreased from -15.94‰ (-17.16‰ to -14.24‰ IQR) to -16.55‰ (-18.65‰ to -15.00‰ IQR) and δ^2H values decreased from -132.60‰ (-137.51‰ to -122.68‰ IQR) to -133.49‰ (-140.94‰ to -123.94‰ IQR) (Figure 3). On September 3, some lakes plotted close to the LMWL, indicating that their waters had experienced negligible amounts of evaporation (Figure 3). The median $\delta^{18}O_I$ values increased from -19.47‰ (-20.10‰ to
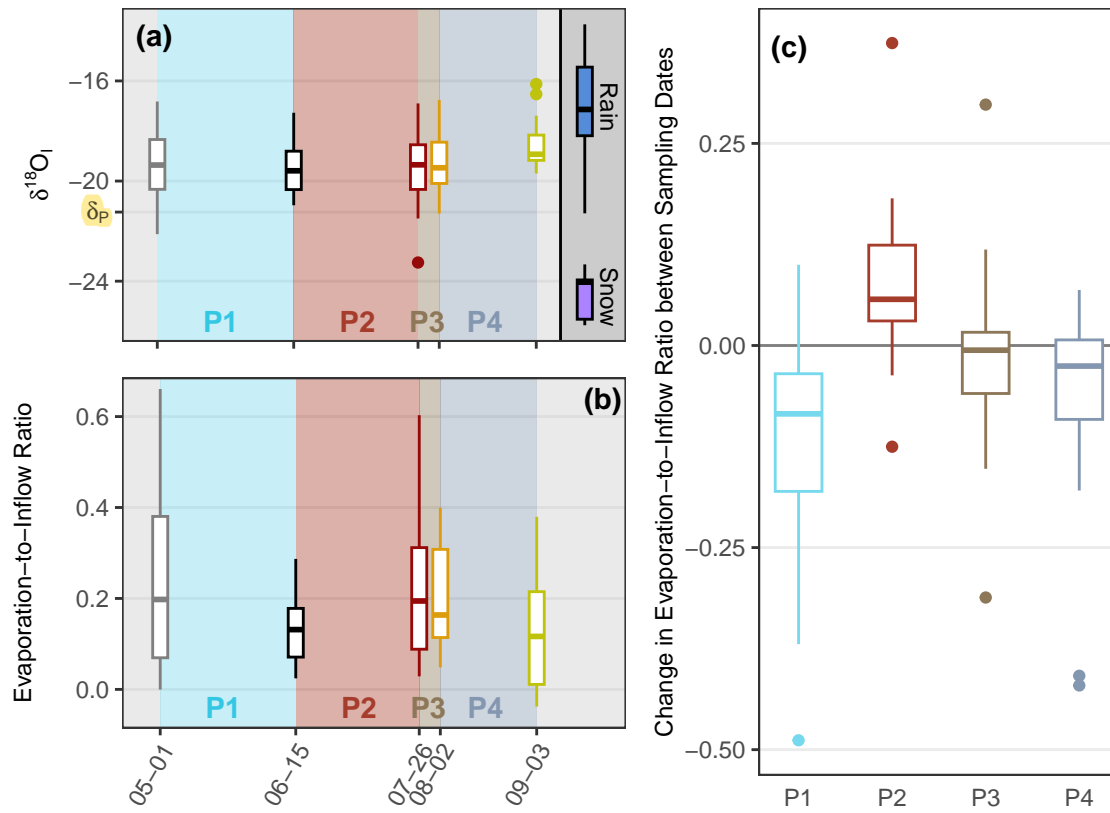
Figure 4. (a) The distribution of $\delta^{18}O_I$ for each sampling date with rain and snow ~samples~ isotope compositions for reference. (b) The distribution of E/I values at all lakes across the ~four~ five sampling dates. (c) The ~distribution of~ lake-specific change in E/I between the sampling dates was calculated as $\Delta[E/I] = [E/I]_{t_2}^{Ln} - [E/I]_{t_1}^{Ln}$, where Ln represents a specific lake, and t represents a sampling date.

230 -18.45‰ IQR) to -18.94‰ (-19.18‰ to -18.14‰ IQR) and the range of values narrowed and became more similar to rain (Figure 4a). Median E/I values also returned towards June 15 values by the end of P4, decreasing to a median of 0.11 (0.00 to 0.21 IQR) (Figure 4b). Two thirds of the lakes experienced a decrease in E/I and the median change in E/I was -0.03 (-0.09 to 0.01 IQR) (Figure 4c).

4.2   Correlation analysis between lake and watershed attributes and lake water balance metrics

235 While a distinct seasonal trend was observed in lake water isotope composition, E/I, and $\delta^{18}O_I$, variability Variability among lakes in average E/I and $\delta^{18}O_I$ was partially explained by statistically significant relationships with lake and watershed properties. Average E/I was negatively correlated with WA/LA (p < 0.0001, Table 2, Figure 5a) and average watershed slope (p = 0.0085, Table 2) and was positively correlated with the log of lake surface area (p < 0.0001, Table 2). Thus, lakes that had higher E/I values tended to have relatively smaller watershed size, have a flatter watershed, and be larger in surface area. When these three variables are combined into a

Table 2. Significant correlations between $\delta^{18}O_I$, E/I, and explanatory variables. In cases where there are multiple explanatory variables, the p-values for each explanatory variable are listed respectively. Adjusted R^2 was used in order to control for the tendency of R^2 to increase as explanatory variables are added to a model (Yin and Fan, 2001). Adjusted R^2 was calculated as $R^2_{adj} = 1 - (1 - R^2) * ((n-1)/(n - m - 1))$, where n is the sample size and m is the number of explanatory variables. p-values >0.05 are *italicized*.

Response Variable	Explanatory Variable(s)	p-value(s)	Adjusted R^2
Average E/I	log(WA/LA)	<0.0001	0.7361
Average E/I	log(Lake Area)	<0.0001	0.5092
Average E/I	Average Watershed Slope	0.0085	0.2332
Average E/I	log(WA/LA) + log(Lake Area) + Average Watershed Slope	0.0002, *0.1949*, *0.8472*	0.7339
Average Watershed Slope	log(Lake Area)	0.0040	0.2771
log(WA/LA)	log(Lake Area)	<0.0001	0.5150
log(WA/LA)	Average Watershed Slope	0.0022	0.3128
Average $\delta^{18}O_I$ (‰)	Lake Latitude	0.0027	0.3010
Average $\delta^{18}O_I$ (‰)	Lake Elevation	0.0029	0.2954
Lake Elevation	Lake Latitude	<0.0001	0.9695

240 linear model, only WA/LA remained a significant predictor of average E/I (p = 0.0002) while lake area (p = 0.1949) and average watershed slope (p = 0.8472) became insignificant effects (Table 2). Both lake surface area and average watershed slope were correlated with WA/LA (Table 2). For the relationship between average E/I and WA/LA, the majority of downstream lakes were outliers, having higher than typical E/I ratios for a given WA/LA as they inherited evaporated waters from upstream waterbodies (Figure 5a).

245   Average $\delta^{18}O_I$ was only correlated with two attributes: lake elevation (p = 0.0029) and latitude (p = 0.0027) (Table 2). Lakes at lower elevations and higher latitudes tended to have higher $\delta^{18}O_I$ values (Figure 5b). Lake elevation and latitude are also nearly perfectly correlated (R^2 = 0.97, Table 2), with lake elevation decreasing as latitude increases.

5 Discussion

5.1 Influence of meteorological conditions on lake water balances

250 Water isotope measurements from five discrete time points provide context for characterizing the seasonal evolution of thermokarst lake water balances as a series of phases in relation to meteorological conditions and influential hydrological processes (Figure 6). A previous study at many of the same lakes by Wilcox et al. (2022) observed the presence of snowmelt bypass (Henriksen and Wright, 1977; Hendrey et al., 1980; Bergmann and Welch, 1985; Wilcox et al., 2022) during the Freshet Phase (P1; Figure 6). Initial snowmelt runoff flowing into lakes did not mix with water underneath lake ice because the ~0°C snowmelt

255 runoff was less dense than the deeper, warmer waters beneath the lake ice, causing it to flow into and out of lakes without
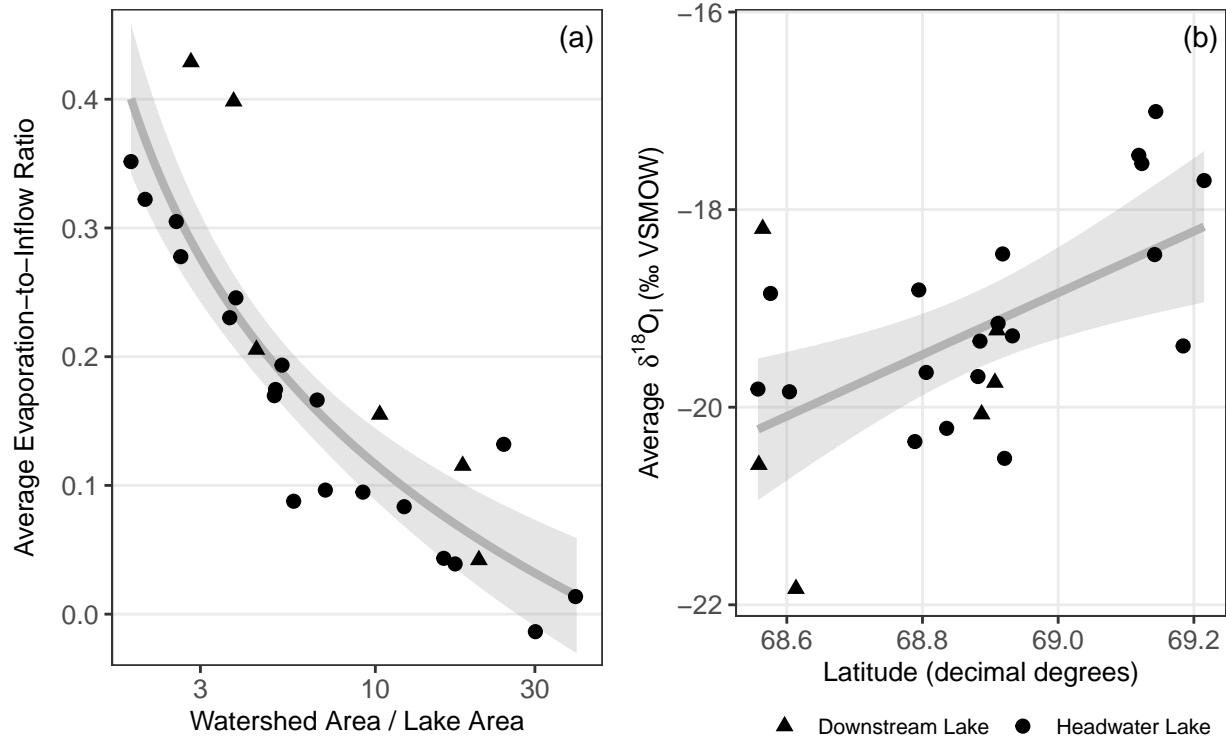
Figure 5. (a) Relationship between average ~~evaporation/inflow~~ evaporation-to-inflow ratio and watershed area/lake area for sampled lakes. The grey line represents a line of best fit between watershed area/lake area and the average ~~evaporation/inflow~~ evaporation-to-inflow ratio, such that $y = \log(x)$, with the 95% confidence interval shown in grey shading ($R^2 = 0.74$, p <0.0001). Note the logarithmic x-axis. (b) The relationship between latitude and δ_I. The grey line represents a linear line of best fit between δ_I and latitude, with the 95% confidence interval shown in grey shading ($R^2 = 0.30$, p = 0.0027).

mixing with lake water(Henriksen and Wright, 1977; Hendrey et al., 1980; Bergmann and Welch, 1985; Wilcox et al., 2022). This resulted in a much smaller reduction in E/I than would have occurred if freshet runoff was able to mix with the entire lake water column(Wilcox et al., 2022). While snowmelt bypass does limit the recharge of lake waters during the Freshet Phase, the sheer volume of snowmelt runoff and lack of evaporation due to lake ice cover ~~results~~ appears to compensate for the impact of snowmelt bypass and results in a

260   greater reduction in E/I ~~greater~~ than any other period (Figure 4c).

During the Freshet Phase, $\delta^{18}O_I$ shifted towards the value of δ_P and not towards δ_S even though minimal rainfall fell during the period (Figure 2) and snowmelt runoff was flowing into lakes. Wilcox et al. (2022) determined that by the time snowmelt runoff could mix with lake waters, the soil had begun to thaw and allowed snowmelt runoff to mix with soil water from the previous year before flowing into lakes. This resulted in a post-snowmelt $\delta^{18}O_I$ that was a mixture of snow-sourced and rain-

265   sourced water (Figure 4a). Since only a small amount of snow-sourced water was incorporated into lakes during the Freshet Phase, the $\delta^{18}O_I$ of lakes remained primarily rain-sourced throughout the entire study period (Figure 4a).
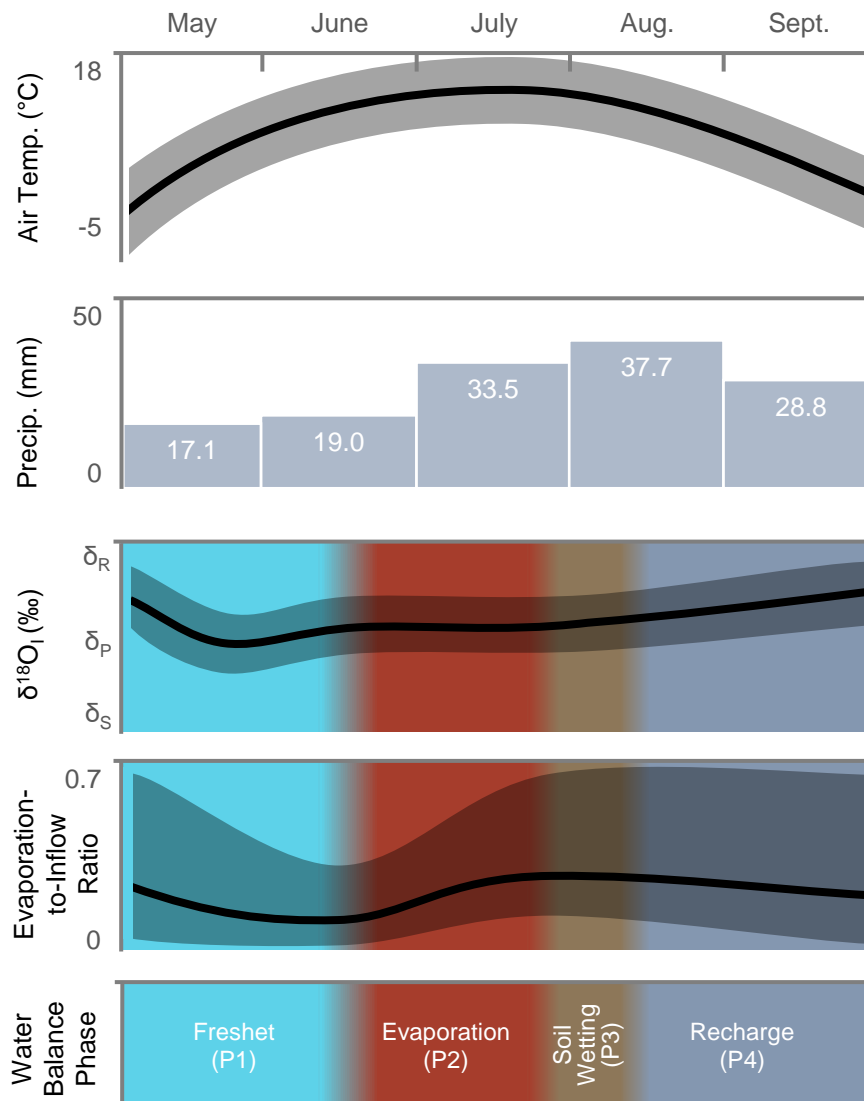
Figure 6. ~~Relations~~ A simplified conceptual diagram ~~showing the connections between~~ meteorological conditions and the response of $\delta^{18}O_I$ and E/I used to designate water balance phases. Air temperature and precipitation data represent average values from 1980-2020. Shaded areas around the $\delta^{18}O_I$ and E/I lines represent the potential variability caused by lake and watershed attributes or meteorological conditions.

The Evaporation Phase (P2; Figure 6) was characterized by minimal change in $\delta^{18}O_I$ (Figure 4a) and rising E/I ratios at nearly all lakes (Figure 4c), caused by the relatively dry and warm conditions that are typical for this region. Previous water balance studies conducted in this region also found that lake evaporation rates were higher as a result of substantial incoming solar radiation in June and July compared to August and September, and when inflow is minimal due to low precipitation (Marsh and Bigras, 1988; Pohl et al., 2009).

During the brief Soil Wetting Phase (P3; Figure 6), there was minimal change in $\delta^{18}O_I$ (Figure 4a) and E/I (Figure 4b) despite the 41.2 mm of rainfall, which represented 25% of the rainfall during the study period. This evidence suggests little runoff was generated by this event and that rainfall that fell directly on lakes had only a minor effect on lake water balances. We hypothesize that dry conditions preceding the rainfall event allowed soils to absorb the rainfall without becoming saturated sufficiently to generate much lateral flow. The lack of runoff in response to this rainfall event is expected given that antecedent soil moisture conditions have been observed to greatly influence the efficiency of runoff generation from rainfall events in areas underlain by continuous permafrost (Roulet and Woo, 1988; Kane et al., 1998; Favaro and Lamoureux, 2014; Stuefer et al., 2017). Since the first half of the summer is typically drier than the second half (Figure 6), soils generally experience drying throughout the first half of the summer before becoming rewetted.

The Recharge Phase (P4; Figure 6) was defined by the $\delta^{18}O_I$ of lakes becoming more similar to rainfall (Figure 4a) and E/I ratios decreasing to values similar to the beginning of the Freshet Phase (Figure 4b). The Recharge Phase of 2018 was 3.8°C lower than average and 66.1 mm of precipitation, exceeding the long-term mean of 37.2 mm (Figure 2). Given the lower air temperatures, it is likely that evaporation rates also decreased and contributed to the decrease in E/I. Since the meteorological conditions were wetter and cooler than the long-term means, we expect the water balance conditions of the Recharge Phase captured in 2018 to be more representative of a later sampling date during a more normal climate year (e.g., late September). E/I ratios on May 1 were greater than September 3, suggesting that lakes received less inflow during the Recharge Phase during 2017 than during 2018 (Figure 4b).

Findings from previous studies of thermokarst lakes in this region imply that the four phases of lake water balance we observed are typical for this region. The four phases of seasonal water balance evolution we identified (Freshet, Evaporation, Soil Wetting, Recharge) roughly follow the pattern of seasonal changes in lake surface area observed by Cooley et al. (2019) who analyzed near-weekly satellite imagery of a large region which encompassed the lakes we studied. Cooley et al. (2019) observed initial decreases in total lake surface area during the Evaporation Phase, followed by stabilizing or increasing trends in lake surface area by the end of August. Additionally, Pohl et al. (2009) modeled the water balance for a single lake in our study region across a 30-year period, and identified that maximum lake level was most likely to occur in early June or late August/early September, corresponding with the start of the Evaporation Phase and end of the Recharge Phase.

In comparison to the five thermokarst lake regions examined in a synthesis of isotope data by MacDonald et al. (2017), the relatively low E/I ratios and rainfall-like $\delta^{18}O_I$ values found at our study lakes compare most closely to lakes in the Alaskan Coastal Plain (ACP), where the majority of lakes also have an E/I < 0.25 and $\delta^{18}O_I$ similar to rain. This region is cooler during the summer and has a shorter ice-free season (Arp et al., 2015) than our study region, but receives less precipitation and is more lake rich (MacDonald et al., 2017), suggesting lakes likely have smaller watersheds than in our study region. The

cooler and shorter summers in ACP, which decrease evaporation, may be offset by smaller watersheds and less precipitation, which decrease inflow, leading to similar E/I values as our study region. Our lakes differed from the more nearby OCF, where most lakes have an E/I between 0.25 and 0.75 but have a smaller WA/LA of ~3, whereas the average WA/LA of lakes we sampled was 9.5 (Table 1). OCF differs from our study region in that it is situated in a post-glacial lake bed underlain by fine-grained glaciolacustrine sediments (Hughes, 1972), resulting in a relatively flat landscape with poorer ability to convey runoff in comparison to our study region, where rolling hills are well drained by networks of peat channels with high hydraulic conductivity (Quinton and Marsh, 1998). These differences between OCF and our study region may explain the greater E/I values at the former, however our study year was cooler and wetter than average, which may also have contributed to the comparatively low E/I ratios.

5.2 Effects of lake and watershed attributes on E/I

While shifts in E/I over time can be attributed to changing meteorological conditions and hydrological processes, differences in E/I among lakes can be further explained by lake and watershed attributes. Most of the variability in average E/I among lakes can be explained by WA/LA (R^2 = 0.74, Figure 5a), as lakes with smaller WA/LA likely receive less inflow and have greater E/I ratios as a result. A similar inverse relationship between E/I ratios and WA/LA has also been observed in OCF (Turner et al., 2014), and the taiga-shield of the Northwest Territories (Gibson and Edwards, 2002). Four of the six downstream lakes we sampled had anomalously high E/I ratios compared to their WA/LA (Figure 5a). Downstream lakes receive evaporated inflow from their upstream lakes, which is then evaporated further in the downstream lake, producing an enhanced E/I ratio. When downstream lakes are removed from the regression between E/I and WA/LA, the R^2 improves from 0.74 to 0.82.

We estimated E/I for all lakes in the study area using the strong relationship between average E/I and WA/LA. This was done by delineating the watersheds of all lakes larger than 0.25 ha in the study area (Figure 1) and applying the fitted regression between log(WA/LA) and average E/I for the headwater lakes we sampled:

$$Average E/I = -0.10867 * \log(WA/LA) + 0.37007 \tag{3}$$

The resulting histogram of average E/I (Figure 7b) is primarily skewed towards larger values, because WA/LA is skewed towards smaller values (Figure 7a). An average E/I between 0.2 and 0.225 is most common for lakes, indicating the lakes are dominated by inflow. At WA/LA >30, the estimated E/I becomes 0, and as a result 7% of lakes are predicted to have an average E/I of 0 (Figure 7b). None of the lakes appear to be approaching desiccation.

We note that this distribution of E/I values is dependent on the timing of our water sampling, the meteorological conditions present during the study period, and on the properties of the lakes that we selected. For example, the median lake depth of 34 lakes sampled in this region by Pienitz et al. (1997) was 3.0 m, similar to the lakes we measured (Table 1), however some lakes sampled by Pienitz et al. (1997) were up to 18.5 m in depth. The relationship we derived between WA/LA and E/I would likely weaken if deeper lakes had been sampled in our study, since lake surface area becomes less representative of lake volume when a wider range of lake depths are included. In that case, calculating the ratio of lake volume to watershed area could be a better predictor of E/I ratios.
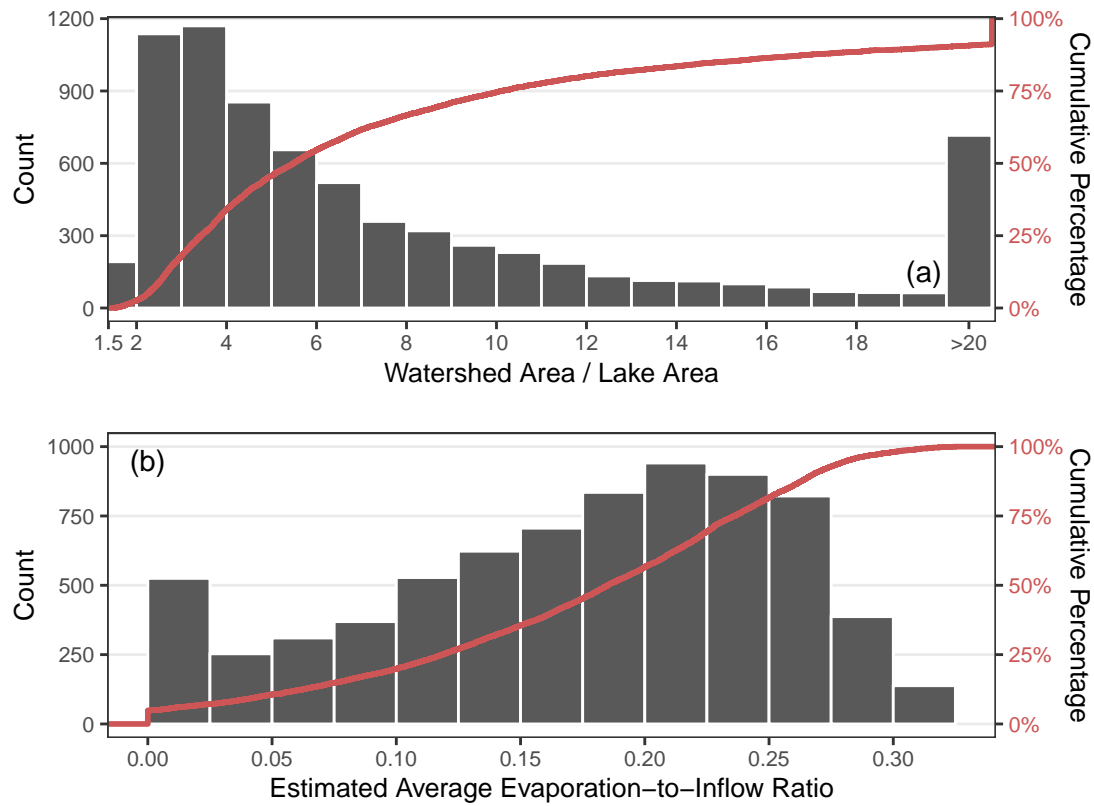
Figure 7. Distribution of (a) watershed area/lake area and (b) evaporation/inflow evaporation-to-inflow for 7340 lakes and their watersheds in the study area. Average evaporation/inflow evaporation-to-inflow is estimated using the relationship with watershed area/lake area of headwater lakes. Note that the leftmost bin in panel (a) is only half the width of other bins, reflecting the rejection of all WA/LA <1.5 that we applied when filtering the data.

335   We hypothesize that the hydrological response of lakes in this region to climate change will be strongly influenced by their WA/LA. Recent predictions of future Arctic precipitation indicate greater rainfall, snowfall and more yearly annual precipitation overall (Brown and Mote, 2009; Bintanja and Andry, 2017; Bintanja et al., 2020) and in OCF increased rainfall is already reducing lake E/I ratios (MacDonald et al., 2021). We would expect that under wetter conditions E/I ratios would decrease for all lakes, and the threshold where average E/I = 0 would also decrease. The logarithmic nature of the relationship between

340   WA/LA and E/I indicates that average E/I is more sensitive to changes in inflow as WA/LA decreases. Therefore, we expect that lakes with smaller WA/LA would experience greater reductions in average E/I under a wetter future climate. We also hypothesize that lakes with larger WA/LA could be more vulnerable to rapid lake drainage because they receive more inflow and likely experience greater fluctuations in lake level as a result; rapid drainage is typically triggered when extremely high water levels lead to the rapid thermo-mechanical erosion of a new lake outlet (Mackay, 1988; Brewer et al., 1993; Turner et al.,

345   2010).

Alternatively, climate change may lead to a drier future for lakes, as ice-free periods lengthen, warmer air temperatures increase evaporation and permafrost thaw leads to landscape drying (Walvoord and Kurylyk, 2016; Koch et al., 2022)(Walvoord and Kurylyk, 2016; Koch et al., 2022; Webb and Liljedahl, 2023). A combination of such conditions have has already caused lake contraction in western Greenland (Finger Higgens et al., 2019). If drier conditions prevail, given the logarithmic nature of the relationship between WA/LA and average E/I, we expect lakes with smaller WA/LA will experience greater increases in average E/I. If future climate change causes dry enough sufficiently dry conditions to cause lake desiccation, a large number of lakes in the study area could potentially be affected, given that the distribution of WA/LA in the region is skewed towards smaller values of WA/LA, with many lakes possessing a WA/LA <4 (Figure 7a). The 'drier future' scenario may seem less likely to result in lake desiccation given that lakes are currently dominated by inflow, however the portion of precipitation converted into runoff can be halved during dry periods when compared to wetter periods (Stuefer et al., 2017), further reducing runoff to lakes.

Future studies could build on our hypothesis that WA/LA will mediate the response of lakes to climate change by comparing past changes in lake surface area, via remote sensing and paleohydrological analyses, with WA/LA. We would expect that during drier periods, lakes with smaller WA/LA experienced greater reductions in lake surface area than lakes with larger WA/LA. Previous studies from this region have already found that lakes change in surface area in response to seasonal (Cooley et al., 2019) and multi-year (Plug et al., 2008) shifts in precipitation, indicating that changes to lake water balances can be observed by tracking changes in water surface area.

6 Conclusions

Water isotope-derived metrics were used to derive distinct seasonal phases of lake water balances for 25 thermokarst lakes in the tundra uplands east of the Mackenzie Delta (Northwest Territories, Canada). The freshet phase Freshet Phase saw lakes experience a reduction in E/I and a shift of δ_I values towards δ_P, as a mixture of soil water and snowmelt-sourced freshet entered lakes and evaporation was minimal due to lake ice cover. Following this period was the evaporaiton phase Evaporation Phase, where minimal precipitation and warm and sunny conditions lead led to increasing E/I ratios and no change in δ_I. Then, a brief and intense period of rainfall lead led to minimal response in E/I and δ_I at lakes, as dry soils absorbed most of the precipitation during the soil wetting phase Soil Wetting Phase. In the final stages of summer during the recharge phase Recharge Phase, air temperatures dropped declined and precipitation was unseasonably high, causing reductions in E/I and a shift of δ_I towards δ_R as lakes received increased runoff from their watersheds and evaporation rates were reduced.

Comparison of water isotope-derived lake water balance components with lake and watershed attributes shows that WA/LA explains the majority of variability in E/I among lakes. The strong relationship between average E/I and WA/LA allowed us to predict the average E/I for 7340 lakes in the study region. Predicted average E/I values were low compared to other regions of thermokarst lakes, only reaching as high as 0.33, indicating that lakes are not currently near risk of desiccation. We hypothesize that lakes with larger WA/LA will be more prone to rapid drainage if future conditions are wetter.

Few studies have directly investigated the influence of WA/LA on E/I (Gibson and Edwards, 2002; Turner et al., 2014), but given the strong relationship we found, WA/LA could serve as a useful metric in other permafrost environments for charac-

terizing thermokarst lake water balances and predicting which lakes may be vulnerable the vulnerability of lakes to climate change.
The non-uniform response of lake surface area to past climate change (Smith et al., 2005; Plug et al., 2008; Arp et al., 2011; Jones et al., 2011; Andresen and Lougheed, 2015) may also be explained by WA/LA; future studies could investigate whether lakes with smaller WA/LA are more likely to decrease in surface area than lakes with larger WA/LA. Further links associations between WA/LA and biogeochemical properties of lakes may also exist, as E/I has been linked to the biogeochemistry of a wide range of lakes, from tropical to tundra environments (Kosten et al., 2009).

Data availability. Data used in the manuscript are presented in Tables 1, 2 and the Appendix. Lake isotope and attribute data can be downloaded from the Trail Valley Creek Dataverse at https://doi.org/10.5683/SP3/AZE4ER. Meteorological data were retrieved from Environment and Climate Change Canada at https://climate.weather.gc.ca/historical_data/search_historic_data_e.html.

Appendix A: Isotope framework

Table A1. List of variables used in isotope framework and their values.

Variable (unit)	Description	Source	Value(s)
Measured			
T (K)	Average air temperature from June 15 to September 3, 2018	Trail Valley Creek (WMO ID: 71683)	281.95
h (%)	Average relative humidity from June 15 to September 3, 2018	Trail Valley Creek (WMO ID: 71683)	78.3
δ_S (^{18}O, ^2H) (‰)	Average isotope composition of snowpack samples.	Samples from study region	-24.61, -184.19
δ_R (^{18}O, ^2H) (‰)	Average isotope composition of rainfall samples.	Samples from study region	-17.03, -129.54
δ_P (^{18}O, ^2H) (‰)	Average of δ_S and δ_R.	Samples from study region	-21.24, -160.1
δ_{Ps} (^{18}O, ^2H) (‰)	Average isotope composition of precipitation during the ice-free period.	Samples from study region	-16.79, -129.15
δ_L (^{18}O, ^2H) (‰)	Isotope composition of lake water.	Samples from study region	*Many*
LMWL (slope, intercept (‰))	Local meteoric water line, calculated using a linear regression through δ_S and δ_R samples.	Samples from study region	7.1, -10.0
Computed			
α^* (^{18}O, ^2H)	Fractionation factor between the liquid and vapour phase of water.	Equation A2, A3	1.0109, 1.0986
ε^* (^{18}O, ^2H)	Equal to $\alpha^* - 1$	Equation A2, A3	0.0109, 0.0986
ε_k (^{18}O, ^2H)	Kinetic separation factor between liquid and vapour phases of water.	Equation A4	3.08, 2.71
δ_{As} (^{18}O, ^2H) (‰)	Isotope composition of atmospheric water vapour.	Equation A5	-27.58, -207.7
δ_E (^{18}O, ^2H) (‰)	Isotope composition of water vapour evaporating from a lake.	Equation A7	*Many*
δ^* (^{18}O, ^2H) (‰)	Theoretical isotope composition of a water body at the point of total desiccation.	Equation A1	-9.88, -101.1
LEL (slope, intercept (‰))	Local evaporation line, representing a theoretical lake evaporation line where $\delta_I = \delta_P$.	Equation A1	5.2, -48.9
δ_I (^{18}O, ^2H) (‰)	Estimated average isotope composition of δ_L source water.	Equation A7	*Many*
E/I	Evaporation-to-inflow ratio.	Equation A8	*Many*
δ_{SSL} (^{18}O, ^2H) (‰)	Isotope composition of a lake where $E/I = 1$ and $\delta_I = \delta_P$.	Equation A6	-12.59, -115.70

The calculation of the point of maximum evaporative isotopic enrichment, or the isotope composition of lake at the point of desiccation (δ^*), Gonfiantini (1986):

$$\delta^* = \frac{h * \delta_{As} + \varepsilon_k + (\varepsilon^*/\alpha^*)}{h - \varepsilon_k - (\varepsilon^*/\alpha^*)} \tag{A1}$$

where α^* is the fractionation factor between the liquid and vapour phase of water, ε^* and ε_k are the equilibrium and kinetic separation terms, with ε^* serving as a convenient expression of α^*, where $\varepsilon^* = \alpha^* - 1$. The term h represents the relative humidity for the open water season (see below). Equilibrium fractionation (α^*) was calculated following equations from Horita and Wesolowski (1994):

$$1000 ln * \alpha^* = -7.685 + 6.7123 * \frac{10^3}{T} - 1.6664 * \frac{10^6}{T^2} + 0.35041 * \frac{10^9}{T^3} \tag{A2}$$

for δ^{18}O and

$$1000 ln * \alpha^* = 1158.8 * \frac{T^3}{10^9} - 1620.1 * \frac{T^2}{10^6} + 794.84 * \frac{T}{10^3} - 161.04 + 2.9992 * \frac{10^9}{T^3} \tag{A3}$$

for δ^2H, where T represents the temperature of the interface (K) (see below). The kinetic separation term ε_k was calculated as:

$$\varepsilon_k = x * (1 - h) \tag{A4}$$

where $x = 0.0142$ for δ^{18}O and $x = 0.0125$ for δ^2H (Gonfiantini, 1986). δ_{As} represents the isotope composition of atmospheric vapour, which we assume is in equilibrium with the isotope composition of summertime precipitation (δ_{Ps}, Gibson and Edwards, 2002). We can therefore estimate δ_{As} as:

$$\delta_{As} = (\delta_{Ps} - \varepsilon^*/\alpha^*) \tag{A5}$$

The reference point of when E/I = 1 (δ_{SSL}) was calculated using:

$$\delta_{SSL} = (\alpha^* * \delta_{Ps}P * (1 - h + \varepsilon_k)) + \alpha^* * h * \delta_{As} + \alpha^* * \varepsilon_k + \varepsilon^* \tag{A6}$$

where δ_{Ps} represents summertime precipitation during the open-water season (Gonfiantini, 1986).

Data for air temperature and relative humidity were collected at Trail Valley Creek near the centre of the study area. The time period used for the average air temperature and relative humidity spans from when lakes became ice-free (June 15, 2018) until the last day of sampling (September 3, 2018) to match the time span between the first and last sampling dates. For a few dates, air temperature was not recorded by the TVC meteorological station maintained by the Meteorological Service of Canada, and air temperature from another meteorological station at TVC was used instead.

The isotope composition of the lake-specific input water (δ_I) was calculated following Yi et al. (2008), where δ_I is estimated as the intersection of the LMWL and the lake-specific LEL, defined as the line between the measured isotope composition of the lake (δ_L) and δ_E, which is the isotope composition of vapour evaporating from the lake. δ_E was calculated following Gonfiantini (1986):

$$\delta_E = \frac{(\delta_L - \varepsilon^*)/(\alpha^* - h * \delta_{As} - \varepsilon_k)}{1 - h - \varepsilon_k} \frac{(\delta_L - \varepsilon^*)/(\alpha^* - h * \delta_{As} - \varepsilon_k)}{1 - h + \varepsilon_k} \tag{A7}$$

δ_I, δ_E and δ_L were then used to calculate the ratio of ~~evaporation to inflow~~ evaporation-to-inflow (E/I) as described by Yi et al. (2008) and others as:

$$\frac{E}{I} = \frac{\delta_I - \delta_L}{\delta_E - \delta_L} \tag{A8}$$

assuming that lakes are well mixed and in hydrological and isotopic steady state.

Table A2. Parameters used in isotope framework.

Parameter (unit)	Source	Value(s)
T (K)	Trail Valley Creek (WMO ID: 71683)	281.95
h (%)	Trail Valley Creek (WMO ID: 71683)	78.3
δ_P(^{18}O, ^{2}H) (‰)	Samples from study region.	-21.24,-160.1
δ_{SSL}(^{18}O, ^{2}H) (‰)	Equation A6	-11.65, -108.3
δ^* (18O, 2H) (‰)	Equation A1	-9.88, -101.1
δ_{As} (^{18}O, ^{2}H) (‰)	Equation A5	-27.58, -207.7
α^* (^{18}O, ^{2}H) (‰)	Equation A2, A3	1.0109, 1.0986
ε_k (^{18}O, ^{2}H)	Equation A4	3.08, 2.71

Author contributions. The study design and sampling plan was developed by E.J.W. with input from B.B.W. and P.M. The field data collection and sample preparation for lab analysis was done by E.J.W. Analysis of the data was completed by E.J.W. with input from B.B.W. The manuscript was primarily written by E.J.W. with input from B.B.W. and P.M.

Competing interests. The authors declare that they do not have any conflict of interest.

Acknowledgements. E.J.W was funded by a W. Garfield Weston Award for Northern Research and an Ontario Graduate Scholarship. We acknowledge funding from ArcticNet, Northern Scientific Training Program, Polar Continental Shelf Program, the Canada Research Chairs program, and the Natural Sciences and Engineering Research Council of Canada. The research license (No. 16237) was administered by the Aurora Research Institute in Inuvik, Northwest Territories, Canada, and can be found at http://data.nwtresearch.com/Scientific/16237. The authors are grateful for the assistance of the Arctic Hydrology Research Group members for their help in completing the field work. The authors also thank the staff of the UW-EIL for completing the isotope analyses, and Rhys Gwynne for providing details about the isotope analysis protocol.

References

435   Andresen, C. G. and Lougheed, V. L.: Disappearing Arctic tundra ponds: Fine-scale analysis of surface hydrology in drained thaw lake basins over a 65 year period (1948-2013), Journal of Geophysical Research: Biogeosciences, 120, 466–479, https://doi.org/10.1002/2014JG002778, 2015.

Arp, C. D., Jones, B. M., Urban, F. E., and Grosse, G.: Hydrogeomorphic processes of thermokarst lakes with grounded-ice and floating-ice regimes on the Arctic coastal plain, Alaska, Hydrological Processes, 25, 2422–2438, https://doi.org/10.1002/hyp.8019, 2011.

440   Arp, C. D., Jones, B. M., Liljedahl, A. K., Hinkel, K. M., and Welker, J. A.: Depth, ice thickness, and ice-out timing cause divergent hydrologic responses among Arctic lakes, Water Resources Research, 51, 9379–9401, https://doi.org/10.1016/0022-1694(68)90080-2, 2015.

Bartsch, A., Widhalm, B., Leibman, M., Ermokhina, K., Kumpula, T., Skarin, A., Wilcox, E. J., Jones, B. M., Frost, G. V., Höfler, A., and Pointner, G.: Feasibility of tundra vegetation height retrieval from Sentinel-1 and Sentinel-2 data, Remote Sensing of Environment, 237,

445   111 515, https://doi.org/10.1016/j.rse.2019.111515, 2020.

Bergmann, M. A. and Welch, H. E.: Spring Meltwater Mixing in Small Arctic Lakes, Canadian Journal of Fisheries and Aquatic Sciences, 42, 1789–1798, https://doi.org/10.1139/f85-224, 1985.

Bintanja, R. and Andry, O.: Towards a rain-dominated Arctic, Nature Climate Change, 7, 263–267, https://doi.org/10.1038/nclimate3240, 2017.

450   Bintanja, R., van der Wiel, K., van der Linden, E. C., Reusen, J., Bogerd, L., Krikken, F., and Selten, F. M.: Strong future increases in Arctic precipitation variability linked to poleward moisture transport, Science Advances, 6, eaax6869, https://doi.org/10.1126/sciadv.aax6869, 2020.

Bouchard, F., Turner, K. W., MacDonald, L. A., Deakin, C., White, H., Farquharson, N., Medeiros, A. S., Wolfe, B. B., Hall, R. I., Pienitz, R., and Edwards, T. W. D.: Vulnerability of shallow subarctic lakes to evaporate and desiccate when snowmelt runoff is low, Geophysical

455   Research Letters, 40, 6112–6117, https://doi.org/10.1002/2013GL058635, 2013.

Brewer, M. C., Carter, L., Glenn, R., and Murray, R.: Sudden drainage of a thaw lake on the Alaskan Arctic coastal plain, in: Proceedings of the Sixth International Conference on Permafrost, pp. 48–53, Wushan Guangzhou: South China University of Technology Press, 1993.

Brock, B. E., Yi, Y., Clogg-Wright, K. P., Edwards, T. W. D., and Wolfe, B. B.: Multi-year landscape-scale assessment of lakewater balances in the Slave River Delta, NWT, using water isotope tracers, Journal of Hydrology, 379, 81–91, https://doi.org/10.1016/j.jhydrol.2009.09.046,

460   2009.

Brown, R. D. and Mote, P. W.: The response of Northern Hemisphere snow cover to a changing climate, Journal of Climate, 22, 2124–2145, https://doi.org/10.1175/2008JCLI2665.1, 2009.

Burn, C. and Kokelj, S.: The Environment and Permafrost of the Mackenzie Delta Area, Permafrost and Periglacial Processes, 20, 83–105, https://doi.org/10.1002/ppp, 2009.

465   Cooley, S. W., Smith, L. C., Ryan, J. C., Pitcher, L. H., and Pavelsky, T. M.: Arctic-Boreal Lake Dynamics Revealed Using CubeSat Imagery, Geophysical Research Letters, 46, 2111–2120, https://doi.org/10.1029/2018GL081584, 2019.

Coplen, T. B.: New guidelines for reporting stable hydrogen, carbon, and oxygen isotope-ratio data, Geochimica et Cosmochimica Acta, 60, 3359–3360, 1996.

Craig, H.: Isotopic Variations in Meteoric Waters, Science, 133, 1702–1703, https://doi.org/10.1126/science.133.3465.1702, 1961.

470   Edwards, T. W. D., Wolfe, B. B., Gibson, J. J., and Hammarlund, D.: Use of water isotope tracers in high latitude hydrology and paleohydrology, in: Long-term Environmental Change in Arctic and Antarctic Lakes, edited by Smol, J. P., Pienitz, R., and Douglas, M. S. V., vol. 8 of *Developments in Paleoenvironmental Research*, pp. 187–207, Springer Netherlands, Dordrecht, https://doi.org/10.1007/978-1-4020-2126-8_7, 2004.

Environment and Climate Change Canada: Historical Climate Data, https://climate.weather.gc.ca/climate_data/daily_data_e.
475   html?hlyRange=2003-08-07%7C2023-02-21&dlyRange=2003-08-01%7C2023-02-21&mlyRange=2003-08-01%7C2007-11-01& StationID=41883&Prov=NT&urlExtension=_e.html&searchType=stnName&optLimit=yearRange&StartYear=1840&EndYear=2022& selRowPerPage=25&Line=4&searchMethod=contains&Month=1&Day=2&txtStationName=inuvik&timeframe=2&Year=2018, 2019.

ESRI: ArcGIS 10.7.1, 2019.

Essery, R. and Pomeroy, J.: Vegetation and Topographic Control of Wind-Blown Snow Distributions in Distributed and Ag-
480   gregated Simulations for an Arctic Tundra Basin, Journal of Hydrometeorology, 5, 735–744, https://doi.org/10.1175/1525-7541(2004)005<0735:VATCOW>2.0.CO;2, 2004.

Favaro, E. A. and Lamoureux, S. F.: Antecedent Controls on Rainfall Runoff Response and Sediment Transport in a High Arctic Catchment, Geografiska Annaler: Series A, Physical Geography, 96, n/a–n/a, https://doi.org/10.1111/geoa.12063, 2014.

Ferrick, M. G., Calkins, D. J., Perron, N. M., Cragin, J. H., and Kendall, C.: Diffusion model validation and interpretation of stable isotopes
485   in river and lake ice, Hydrological Processes, 16, 851–872, https://doi.org/10.1002/hyp.374, 2002.

Finger Higgens, R. A., Chipman, J. W., Lutz, D. A., Culler, L. E., Virginia, R. A., and Ogden, L. A.: Changing Lake Dynamics Indicate a Drier Arctic in Western Greenland, Journal of Geophysical Research: Biogeosciences, 124, 870–883, https://doi.org/10.1029/2018JG004879, 2019.

Fritz, M., Wetterich, S., McAlister, J., and Meyer, H.: A new local meteoric water line for Inuvik (NT, Canada), Earth System Science Data,
490   14, 57–63, https://doi.org/10.5194/essd-14-57-2022, 2022.

Gibson, J.: Short-term evaporation and water budget comparisons in shallow Arctic lakes using non-steady isotope mass balance, Journal of Hydrology, 264, 242–261, https://doi.org/10.1016/S0022-1694(02)00091-4, 2002.

Gibson, J. J. and Edwards, T. W. D.: Regional water balance trends and evaporation-transpiration partitioning from a stable isotope survey of lakes in northern Canada, Global Biogeochemical Cycles, 16, 10–11, https://doi.org/doi: 10.1029/2001GB001839, 2002.

495   Gibson, J. J., Edwards, T. W. D., and Bursey, G. G.: Estimating Evaporation Using Stable Isotopes : Quantitative Results and Sensitivity Analysis for Two Catchments in Northern Canada, Nordic Hydrology, 24, 79–94, https://doi.org/10.2166/nh.1993.006, 1993.

Gonfiantini, R.: Environmental Isotopes in Lake Studies, in: The Terrestrial Environment, B, pp. 113–168, Elsevier, https://doi.org/10.1016/B978-0-444-42225-5.50008-5, 1986.

Grünberg, I., Wilcox, E. J., Zwieback, S., Marsh, P., and Boike, J.: Linking tundra vegetation, snow, soil temperature, and permafrost,
500   Biogeosciences, 17, 4261–4279, https://doi.org/10.5194/bg-17-4261-2020, 2020.

Hendrey, G. R., Galloway, J. N., and Schofield, C. L.: Temporal and spatial trends in the chemistry of acidified lakes under ice cover., in: International Conference on the Ecological Impact of Acid Precipitation, Brookhaven National Lab, 1980.

Henriksen, A. and Wright, R. F.: Effects of Acid Precipitation on a Small Acid Lake in Southern Norway, Nordic Hydrology, 8, 1–10, https://doi.org/10.2166/nh.1977.0001, 1977.

505   Horita, J. and Wesolowski, D. J.: Liquid-vapor fractionation of oxygen and hydrogen isotopes of water from the freezing to the critical temperature, Geochimica et Cosmochimica Acta, 58, 3425–3437, https://doi.org/10.1016/0016-7037(94)90096-5, 1994.

Hughes, O. L.: Surficial Geology of northern Yukon Territory and northwestern District of Mackenzie, Northwest Territories, Tech. rep., https://doi.org/10.4095/102354, 1972.

IAEA/WMO: Global Network of Isotopes in Precipitation, The GNIP Database [data set], https://nucleus.iaea.org/wiser, 2023.

510 Jones, B. M., Grosse, G., Arp, C. D., Jones, M. C., Walter Anthony, K. M., and Romanovsky, V. E.: Modern thermokarst lake dynamics in the continuous permafrost zone, northern Seward Peninsula, Alaska, Journal of Geophysical Research, 116, G00M03, https://doi.org/10.1029/2011JG001666, 2011.

Kane, D. L., Soden, D. J., Hinzman, L. D., and Gieck, R. E.: Rainfall runoff of a nested watershed in the alaskan arctic, in: Seventh International Conference on Permafrost, 55, pp. 539–544, Nordicana, Yellowknife, 1998.

515 Koch, J. C., Sjoberg, Y., O'Donnell, J., Carey, M., Sullivan, P. F., and Terskaia, A.: Sensitivity of headwater streamflow to thawing permafrost and vegetation change in a warming Arctic, Environmental Research Letters, 2, 0–31, https://doi.org/10.1088/1748-9326/ac5f2d, 2022.

Kosten, S., Huszar, V. L., Mazzeo, N., Scheffer, M., Sternberg, L. d. S., and Jeppesen, E.: Lake and watershed characteristics rather than climate influence nutrient limitation in shallow lakes, Ecological applications, 19, 1791–1804, 2009.

Lantz, T. C., Gergel, S. E., and Kokelj, S. V.: Spatial heterogeneity in the shrub tundra ecotone in the Mackenzie Delta region, Northwest 520 territories: Implications for Arctic environmental change, Ecosystems, 13, 194–204, https://doi.org/10.1007/s10021-009-9310-0, 2010.

MacDonald, L. A., Wolfe, B. B., Turner, K. W., Anderson, L., Arp, C. D., Birks, S. J., Bouchard, F., Edwards, T. W., Farquharson, N., Hall, R. I., McDonald, I., Narancic, B., Ouimet, C., Pienitz, R., Tondu, J., and White, H.: A synthesis of thermokarst lake water balance in high-latitude regions of North America from isotope tracers, Arctic Science, 3, 118–149, https://doi.org/10.1139/as-2016-0019, 2017.

MacDonald, L. A., Turner, K. W., McDonald, I., Kay, M. L., Hall, R. I., and Wolfe, B. B.: Isotopic evidence of increasing water abundance and 525 lake hydrological change in Old Crow Flats, Yukon, Canada, Environmental Research Letters, 16, 124 024, https://doi.org/10.1088/1748-9326/ac3533, 2021.

Mackay, J. R.: Catastrophic lake drainage, Tuktoyaktuk Peninsula area, District of Mackenzie, in: Current research part D: interior plains and Arctic Canada, pp. 83–90, Geological Survey of Canada, https://doi.org/10.4095/122651, 1988.

Marsh, P. and Bigras, S. C.: Evaporation from Mackenzie Delta Lakes, N.W.T., Canada, Arctic and Alpine Research, 20, 220, 530 https://doi.org/10.2307/1551500, 1988.

Marsh, P., Russell, M., Pohl, S., Haywood, H., and Onclin, C.: Changes in thaw lake drainage in the Western Canadian Arctic from 1950 to 2000, Hydrological Processes, 23, 145–158, https://doi.org/10.1002/hyp.7179, 2009.

Marsh, P., Mann, P., and Walker, B.: Changing snowfall and snow cover in the western Canadian Arctic, in: 22nd Northern Research Basins Symposium and Workshop, pp. 1–10, Yellowknife, 2019.

535 Narancic, B., Wolfe, B. B., Pienitz, R., Meyer, H., and Lamhonwah, D.: Landscape-gradient assessment of thermokarst lake hydrology using water isotope tracers, Journal of Hydrology, 545, 327–338, https://doi.org/10.1016/j.jhydrol.2016.11.028, 2017.

Nitze, I., Grosse, G., Jones, B. M., Arp, C. D., Ulrich, M., Fedorov, A., and Veremeeva, A.: Landsat-based trend analysis of lake dynamics across Northern Permafrost Regions, Remote Sensing, 9, 1–28, https://doi.org/10.3390/rs9070640, 2017.

O'Callaghan, J. F. and Mark, D. M.: The extraction of drainage networks from digital elevation data, Computer Vision, Graphics, and Image 540 Processing, 28, 323–344, 1984.

PGC: ArcticDEM, https://www.pgc.umn.edu/data/, 2018.

Pienitz, R., Smol, J. P., and Lean, D. R.: Physical and chemical limnology of 59 lakes located between the southern Yukon and the Tuktoyaktuk Peninsula, Northwest Territories (Canada), Canadian Journal of Fisheries and Aquatic Sciences, 54, 330–346, https://doi.org/10.1139/f96-274, 1997.

545   Plug, L. J., Walls, C., and Scott, B. M.: Tundra lake changes from 1978 to 2001 on the Tuktoyaktuk Peninsula, western Canadian Arctic, Geophysical Research Letters, 35, 1–5, https://doi.org/10.1029/2007GL032303, 2008.

Pohl, S., Marsh, P., Onclin, C., and Russell, M.: The summer hydrology of a small upland tundra thaw lake: implications to lake drainage, Hydrological Processes, 23, 2536–2546, https://doi.org/10.1002/hyp.7238, 2009.

Pomeroy, J. W., Bewley, D. S., Essery, R. L. H., Hedstrom, N. R., Link, T., Granger, R. J., Sicart, J. E., Ellis, C. R., and Janowicz, J. R.:

550   Shrub tundra snowmelt, Hydrological Processes, 20, 923–941, https://doi.org/10.1002/hyp.6124, 2006.

Prowse, T., Alfredsen, K., Beltaos, S., Bonsal, B., Duguay, C., Korhola, A., McNamara, J., Pienitz, R., Vincent, W. F., Vuglinsky, V., and Weyhenmeyer, G. A.: Past and future changes in arctic lake and river ice, Ambio, 40, 53–62, https://doi.org/10.1007/s13280-011-0216-7, 2011.

Quinton, W. L. and Marsh, P.: The influence of mineral earth hummocks on subsurface drainage in the continuous permafrost zone, Per-

555   mafrost and Periglacial Processes, 9, 213–228, https://doi.org/10.1002/(SICI)1099-1530(199807/09)9:3<213::AID-PPP285>3.0.CO;2-E, 1998.

R Core Team: R: A Language and Environment for Statistical Computing, https://www.r-project.org/, 2021.

Rampton, V. N.: Quaternary geology of the Tuktoyaktuk coastlands, Northwest Territories, Geological Survey of Canada, 1988.

Remmer, C. R., Owca, T., Neary, L., Wiklund, J. A., Kay, M., Wolfe, B. B., and Hall, R. I.: Delineating extent and magnitude of river flooding

560   to lakes across a northern delta using water isotope tracers, Hydrological Processes, 34, 303–320, https://doi.org/10.1002/hyp.13585, 2020.

Roulet, N. T. and Woo, M. K.: Runoff generation in a low Arctic drainage basin, Journal of Hydrology, 101, 213–226, https://doi.org/10.1016/0022-1694(88)90036-4, 1988.

Smith, L. C., Sheng, Y., MacDonald, G. M., and Hinzman, L. D.: Disappearing Arctic Lakes, Science, 308, 1429–1429, https://doi.org/10.1126/science.1108142, 2005.

565   Stuefer, S. L., Arp, C. D., Kane, D. L., and Liljedahl, A. K.: Recent Extreme Runoff Observations From Coastal Arctic Watersheds in Alaska, Water Resources Research, 53, 9145–9163, https://doi.org/10.1002/2017WR020567, 2017.

Sturm, M., Racine, C., and Tape, K.: Increasing shrub abundance in the Arctic., Nature, 411, 546–547, https://doi.org/10.1038/35079180, 2001.

Tananaev, N. and Lotsari, E.: Defrosting northern catchments: Fluvial effects of permafrost degradation, Earth-Science Reviews, p. 103996,

570   https://doi.org/10.1016/j.earscirev.2022.103996, 2022.

Travers-Smith, H. Z., Lantz, T. C., and Fraser, R. H.: Surface Water Dynamics and Rapid Lake Drainage in the Western Canadian Subarctic (1985–2020), Journal of Geophysical Research: Biogeosciences, 126, e2021JG006445, https://doi.org/10.1029/2021JG006445, 2021.

Turner, K. W., Wolfe, B. B., and Edwards, T. W.: Characterizing the role of hydrological processes on lake water balances in the Old Crow Flats, Yukon Territory, Canada, using water isotope tracers, Journal of Hydrology, 386, 103–117,

575   https://doi.org/10.1016/j.jhydrol.2010.03.012, 2010.

Turner, K. W., Wolfe, B. B., Edwards, T. W. D., Lantz, T. C., Hall, R. I., and Larocque, G.: Controls on water balance of shallow thermokarst lakes and their relations with catchment characteristics: a multi-year, landscape-scale assessment based on water isotope tracers and remote sensing in Old Crow Flats, Yukon (Canada), Global Change Biology, 20, 1585–1603, https://doi.org/10.1111/gcb.12465, 2014.

Walvoord, M. A. and Kurylyk, B. L.: Hydrologic Impacts of Thawing Permafrost—A Review, Vadose Zone Journal, 15, 2–20,

580   https://doi.org/10.2136/vzj2016.01.0010, 2016.

Wan, C., Gibson, J. J., and Peters, D. L.: Isotopic constraints on water balance of tundra lakes and watersheds affected by permafrost degradation, Mackenzie Delta region, Northwest Territories, Canada, Science of the Total Environment, 731, 139 176, https://doi.org/10.1016/j.scitotenv.2020.139176, 2020.

Webb, E. E. and Liljedahl, A. K.: Diminishing lake area across the northern permafrost zone, Nature Geoscience, pp. 1–8, 2023.

585   Wilcox, E. J., Wolfe, B. B., and Marsh, P.: Assessing the influence of lake and watershed attributes on snowmelt bypass at thermokarst lakes, Hydrology and Earth System Sciences, 26, 6185–6205, https://doi.org/10.5194/hess-26-6185-2022, 2022.

Wolfe, B. B., Light, E. M., Macrae, M. L., Hall, R. I., Eichel, K., Jasechko, S., White, J., Fishback, L., and Edwards, T. W.: Divergent hydrological responses to 20th century climate change in shallow tundra ponds, western Hudson Bay Lowlands, Geophysical Research Letters, 38, 1–6, https://doi.org/10.1029/2011GL049766, 2011.

590   Woo, M.-k.: Permafrost Hydrology, Springer Berlin Heidelberg, Berlin, Heidelberg, https://doi.org/10.1007/978-3-642-23462-0, 2012.

Yi, Y., Brock, B. E., Falcone, M. D., Wolfe, B. B., and Edwards, T. W. D.: A coupled isotope tracer method to characterize input water to lakes, Journal of Hydrology, 350, 1–13, https://doi.org/10.1016/j.jhydrol.2007.11.008, 2008.

Yin, P. and Fan, X.: Estimating R^2 Shrinkage in Multiple Regression: A Comparison of Different Analytical Methods, The Journal of Experimental Education, 69, 203–224, https://doi.org/10.1080/00220970109600656, 2001.